JCB Article

# A role for myosin-1A in the localization of a brush border disaccharidase

**Matthew J. Tyska[1] and Mark S. Mooseker[1,2,3]**

[1]Department of Molecular, Cellular, and Developmental Biology, [2]Department of Cell Biology, and [3]Department of Pathology, Yale University, New Haven, CT 06511

To gain insight regarding myosin-1A (M1A) function, we expressed a dominant negative fragment of this motor in the intestinal epithelial cell line, CACO-$2_{BBE}$. Sucrase isomaltase (SI), a transmembrane disaccharidase found in microvillar lipid rafts, was missing from the brush border (BB) in cells expressing this fragment. Density gradient centrifugation, affinity purification, and immunopurification of detergent-resistant membranes isolated from CACO-$2_{BBE}$ cells and rat microvilli (MV) all indicate that M1A and SI reside on the same population of low density (~1.12 g/ml) membranes. Chemical cross-linking of detergent-resistant membranes from rat MV indicates that SI and M1A may interact in a lipid raft complex. The functional significance of such a complex is highlighted by expression of the cytoplasmic domain of SI, which results in lower levels of M1A and a loss of SI from the BB. Together, these studies are the first to assign a specific role to M1A and suggest that this motor is involved in the retention of SI within the BB.

## Introduction

Class I myosins are a group of monomeric actin-based motors that are known to associate with membranes in numerous cell types (Coluccio, 1997). Myosin-1A (M1A) was the first vertebrate myosin I discovered (Mooseker and Cheney, 1995) and is now among the most highly characterized members of this class. Although the biochemical and biophysical properties of purified M1A have been well documented (Hayden et al., 1990; Mooseker and Cheney, 1995; Jontes et al., 1995, 1997), the cellular function of M1A has remained difficult to define. In vivo, M1A localizes to the brush border (BB) of intestinal epithelial cells (IECs); a specialized cytoskeletal domain that consists of tightly packed arrays of microvilli (MV). In these arrays, each MV is supported by a polarized actin bundle that is tethered to the membrane by a helical array of M1A (Mooseker and Cheney, 1995). Thus, M1A might function as a linker required for structural integrity of the MV. Several lines of evidence also suggest that M1A might be involved in the directed movements of intracellular membranes. Fath et al. (1994) first proposed an active role for M1A in the apical targeting of Golgi-derived vesicles based on biochemical studies with membranes from intestinal crypt cells. In addition, the expression of truncated forms of M1A is known to disrupt the distribution and function of the endosomal compartment in unpolarized and polarized cells (Durrbach et al., 1996, 2000). Related motors, myosin-1b and -1c, have also been shown to associate with endosomal and lysosomal vesicles (Raposo et al., 1999) and facilitate the movement of GLUT4 receptors to the plasma membrane in adipocytes (Bose et al., 2002), respectively.

We recently investigated the intramicrovillar dynamics of M1A using the BB-expressing cell line LLC-$PK_1$-CL4 (Tyska and Mooseker, 2002). FRAP measurements on GFP-M1A expressed in CL4 cells showed that ~80% of the population of M1A exchanges rapidly (< 1 min), suggesting that most of the M1A does not function as a static linker within the MV. These studies also showed that the membrane-binding tail domain of M1A is critical for the steady-state localization and turnover kinetics of M1A within the BB. Based on these data, we predicted that overexpression of this fragment in an IEC line might inhibit the function of M1A by displacing it from the BB, generating dominant negative phenotypes and ultimately providing functional insight.

Here, we demonstrate that the BBs of CACO-$2_{BBE}$ (BBE; Peterson and Mooseker, 1992) cells expressing the dominant negative M1A-tail fragment are missing sucrase isomaltase

Address correspondence to Matthew J. Tyska, Department of Molecular, Cellular, and Developmental Biology, Yale University 342 Kline Biology Tower, 266 Whitney Ave., New Haven, CT 06511. Tel.: (203) 432-3469. Fax: (203) 432-6161. email: matthew.tyska@yale.edu

Key words: actin; membrane; lipid raft; microvillus; epithelium

Abbreviations used in this paper: AP, alkaline phosphatase; APN, aminopeptidase N; BB, brush border; BBE, CACO-$2_{BBE}$; ConA, concanavalin A; DRM, detergent-resistant membrane; EDC, 1-ethyl-3-(3-dimethylaminopropyl) carboiimide; IEC, intestinal epithelial cell; IP, immunopurified; MβCD, methyl-β-cyclodextrin; M1A, myosin-1A; MV, microvillus/microvilli; SI, sucrase isomaltase; PAS, protein-A Sepharose; SINT, SI $NH_2$-terminal cytoplasmic domain.

© The Rockefeller University Press, 0021-9525/2004/05/395/11 $8.00

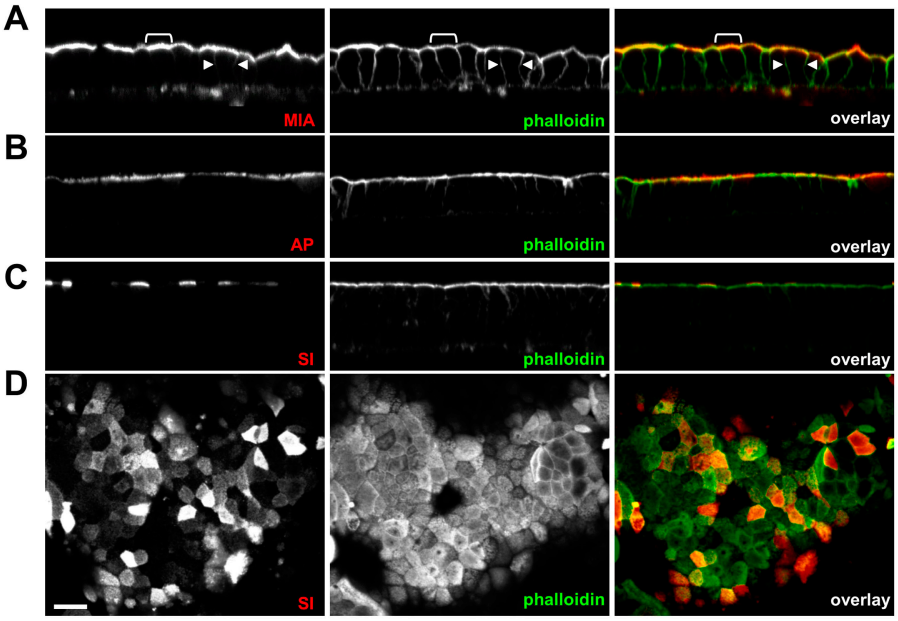


Figure 1. **Localization of endogenous BB components.** Confocal vertical sections of fully differentiated BBE cells demonstrate the endogenous localization of (A) M1A, (B) AP, and (C) SI. The bracket in A highlights the BB from a single cell; arrowheads define the lateral margins. (D) En face confocal section at the level of the BB demonstrates the mosaic nature of SI expression in these cells. In each overlay, the primary signal (red) is shown relative to F-actin (green). Bar, 20 μm.

(SI), a transmembrane disaccharidase known to reside in lipid rafts in the BB membrane (Danielsen, 1995). In vitro, lipid rafts form stable, detergent-resistant membrane (DRM) microdomains (Danielsen and Hansen, 2003). In this report, we provide evidence indicating that M1A is a component of SI-containing DRMs isolated from both BBE cells and rat MV, and further show that these two proteins may interact in a raft complex. The functional significance of this complex is highlighted by expression of the $NH_2$-terminal cytoplasmic domain of SI, which results in lower levels of M1A and a loss of SI from the BB. Together, these studies are the first to assign a specific cellular role to M1A and suggest that this motor is involved in the retention of SI within the BB.

## Results

### BBE cells as a model system for investigating M1A function

When BBE cells are grown at confluency for an extended duration (~3 wk), they differentiate into a highly polarized monolayer with several biochemical and morphological attributes that are reminiscent of native IECs (Peterson and Mooseker, 1992). These include tall, columnar-shaped cells, highly organized BBs with tightly packed MV of uniform length, and the expression and targeting of BB-specific proteins (e.g., villin, M1A, SI, alkaline phosphatase [AP]) in the terminally differentiated state. We used confocal microscopy to examine the distribution of M1A, AP, and SI relative to F-actin (phalloidin) in fully differentiated BBE cells (Fig. 1, A–C). Endogenous M1A, SI, and AP demonstrated intense BB staining along the apical surface of the monolayer (Fig. 1 A, bracket). In addition to staining in the BB domain, M1A also localized to the lateral margins albeit to a lesser extent (Fig. 1 A, arrowheads). The M1A localization observed here is similar to that previously reported in vivo and in BBE cells (Heintzelman and Mooseker, 1990; Peterson and Mooseker, 1992).

### GFP-M1A-tail localizes to the BB domain in BBE cells and results in reduced levels of M1A expression

In an effort to perturb the distribution of native M1A and induce dominant negative phenotypes in BBE cells, we created cell lines stably expressing GFP-M1A-tail (see Materials and methods). Examination of phalloidin-stained BBE

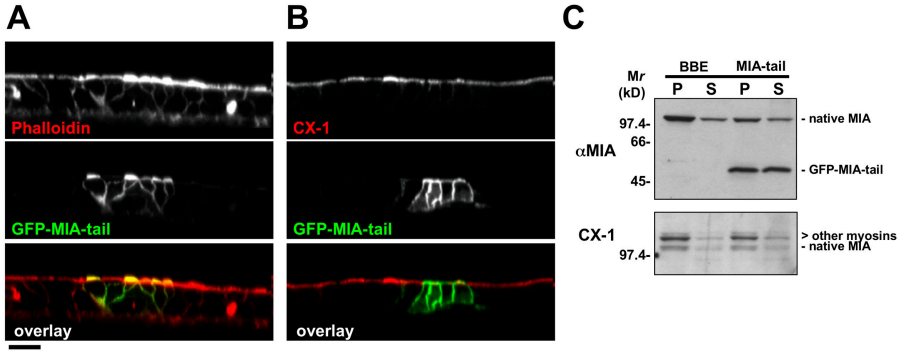


Figure 2. **The expression of GFP-M1A-tail in BBE cells.** Confocal vertical sections of fully differentiated BBE cells demonstrate the localization GFP-M1A-tail relative to the distribution of (A) F-actin or (B) the CX-1 immunogens. In the overlay column, GFP signals are green, whereas phalloidin and CX-1 are pseudo-colored red. Bar, 20 μm. (C) Immunoblots show the distribution of endogenous M1A and GFP-M1A-tail (αM1A) or the CX-1 immunogens in 15,000 *g* pellet (P) and supernatant (S) fractions prepared from BBE cell homogenates in buffer A′ supplemented with 1 mM ATP. The position of native M1A is marked to the right.

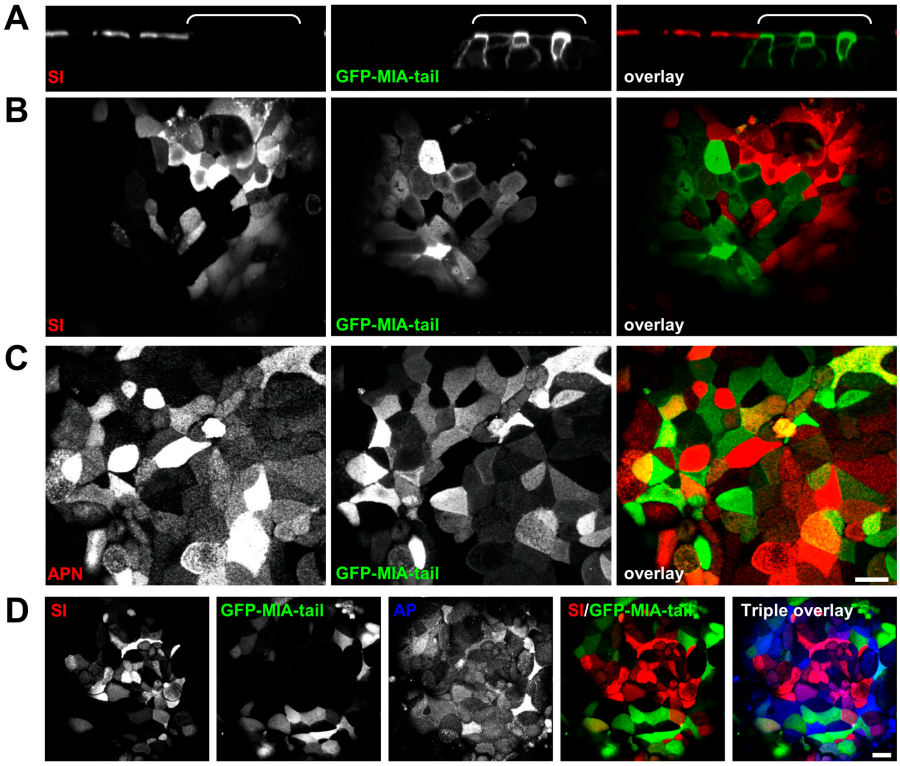


Figure 3. **Distribution of apical membrane markers in BBE cells expressing GFP-M1A-tail.** (A) Vertical and (B) en face confocal sections demonstrate significant defects in SI localization in fully differentiated BBE cells expressing GFP-M1A-tail. The white bracket in (A) highlights a cluster of cells expressing high levels of GFP-M1A-tail and lacking SI localization in the BB. (C) En face confocal section shows that APN localizes in the presence of GFP-M1A-tail. (D) SI and AP double staining reveals that AP localizes properly in cells where GFP-M1A-tail perturbs SI localization. In the overlay images, GFP signals are green, SI and APN are red, AP is blue. Bars, 20 μm.

monolayers expressing GFP-M1A-tail revealed that the strong BB localization and additional lateral signal exhibited by this fusion protein (Fig. 2 A) are similar to that demonstrated by native M1A (Fig. 1 A). These results confirmed our previous report on M1A localization in LLC-PK1-CL4 cells (Tyska and Mooseker, 2002) and indicate that the tail domain of M1A contains significant targeting information.

Because our M1A pAb is tail domain directed, the influence of GFP-M1A-tail expression on endogenous M1A distribution could not be assessed using an immunofluorescence approach. However, densitometric analysis of αM1A immunoblots on 15,000 *g* pellet (P) and supernatant (S) fractions from BBE cells revealed that the total amount of endogenous (P+S) M1A is reduced in GFP-M1A-tail stable lines by ~30% (Fig. 2 C, αM1A). A reduction in the steady-state level of M1A in expressing cells may be indicative of increased turnover resulting from the displacement of this motor from the BB. Given that only a small fraction of the cells in the stable line are expressing GFP-M1A-tail, the actual extent of endogenous M1A suppression per expressing cell is likely much greater. To determine if this effect was specific to M1A or was a general effect on all myosins-I in the BB, we stained BBE cells with an mAb (CX-1) that recognizes multiple myosin-I immunogens in this cell line (Carboni et al., 1988; Peterson and Mooseker, 1992). In cells expressing GFP-M1A-tail, CX-1 immunogens localized to the BB in a normal manner (Fig. 2 B). This finding was confirmed by CX-1 immunoblots where no difference in overall level or distribution of immunogens was detected (Fig. 2 C, CX-1). Because CX-1 recognizes human M1A weakly relative to the other high mol wt immunogens in these blots (Fig. 2 C, CX-1 blot, native M1A), changes in the distribution of M1A (as seen in the αM1A blot) were difficult to detect with this probe. Together, however, these results suggest that any consequence of GFP-M1A-tail expression must be a specific effect on endogenous M1A and not a general effect on other myosins-I in the BB.

## GFP-M1A-tail expression induces SI loss from the BB

Because past studies have implicated M1A in the apical targeting of BB-specific proteins (Fath et al., 1994), we examined GFP-M1A-tail expressing cells for defects in the distribution of apical markers: specifically, the GPI-linked protein, AP, and two type II transmembrane proteins, SI and aminopeptidase N (APN). Inspection of BBE cells expressing GFP-M1A-tail revealed significant perturbations in SI localization (Fig. 3, A and B); SI and GFP-M1A-tail signals appeared mutually exclusive, forming a "lock and key" staining pattern with very little overlap. Cells expressing extremely low levels of GFP-M1A-tail (Fig. 3 A, unbracketed cells) appeared to target SI in a manner similar to the parent line (Fig. 1 C), whereas those expressing higher levels had little or no SI in the BB. This effect was also specific to SI, as distributions of the other apical membrane markers, APN (Fig. 3 C) and AP (Fig. 3 D), appeared normal. Although the expression of SI in parent line BBE cells does appear highly mosaic (Fig. 1 D; Peterson and Mooseker, 1992), the scale of the expression mosaic (variation from cell to cell) is much smaller than the scale of the interruptions we observed due to GFP-M1A-tail expression, where SI localization was perturbed in large fields of cells (Fig. 3, A, B, and D). Because GFP-M1A-tail expression is limited to a small fraction of the cells in these stable lines, Western blotting only revealed a minor reduction in SI levels (~10%; not depicted). However, based on the micrographs in Fig. 3, the true reduction in SI level per cell is probably much greater. Potential mechanisms and implications of SI loss from the BB are discussed in greater detail below (see Discussion).

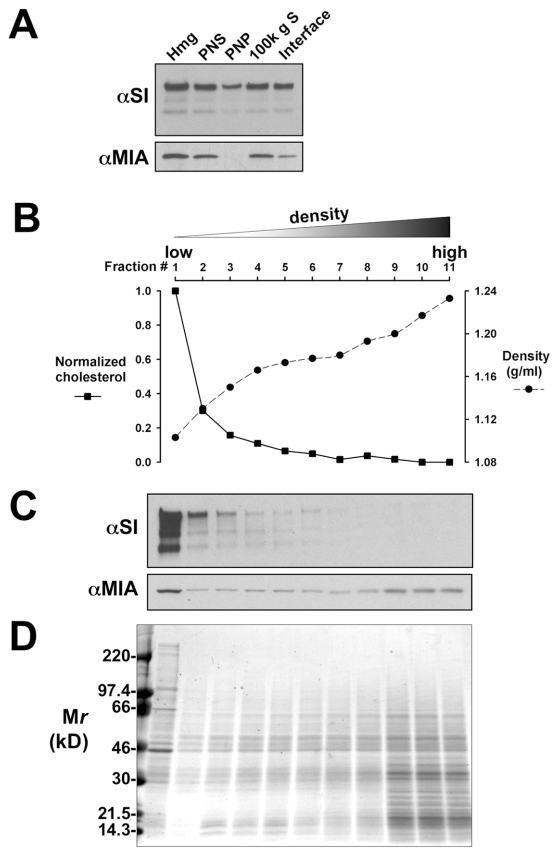


Figure 4. **Characterization of DRMs isolated from BBE cells.** (A) Western blots of fractions from the preparation of crude BBE DRMs (see Materials and methods); Hmg, homogenate; PNS, postnuclear supernatant; PNP, postnuclear pellet; 100 kg S, 100,000 *g* supernatant; interface, the DRM-rich interface (loads are stoichiometric relative to Hmg volume). (B) Density (dashed line, closed circle) and cholesterol (solid line, filled square) profiles of OptiPrep™ gradient fractions. Although these analyses were performed multiple times with similar results, the plots shown here and in other figures are from single, representative experiments. (C) Immunoblots of gradient fractions (loaded for equal volume) probed with antibodies against SI and M1A. (D) Coomassie blue–stained gel demonstrating the protein distribution across gradient fractions; mol wts are indicated on the left.

Although many GFP-M1A-tail expressing cells appeared to have normal BB morphology, a fraction demonstrated significantly stronger phalloidin staining (Fig. 2 A). These potential effects on the actin cytoskeleton may reflect an alternative aspect of M1A function in the BB and will be the focus of future investigation.

## M1A is a component of SI-containing DRMs from BBE cells

SI is an integral membrane disaccharidase that is known to reside in lipid rafts of the BB membrane (Danielsen, 1995). If M1A interacts with SI-containing lipid rafts, then expression of the GFP-M1A-tail fragment could result in the loss of SI from the BB by perturbing M1A-dependent transport or localization of raft structures. In vitro, lipid rafts form stable, low density DRMs (Brown and London, 1998). To determine if M1A is a component of SI-containing DRMs, we isolated crude DRMs from fully confluent BBE cells (see Materials and methods; Fig. 4 A, interface) and performed density gradient analysis. The density profiles (Fig. 4 B, dashed line/filled circles) typically generated by the Optiprep™ gradients used for these studies appeared slightly nonlinear, but were highly reproducible. Immunoblots (Fig. 4 C) of gradient fractions showed that SI and M1A are both enriched in the lowest density (~1.11 g/ml) fraction. The cholesterol profile (Fig. 4 B, solid line/filled squares) of the same gradient revealed that the lowest density fractions also have the highest cholesterol levels, as expected for DRMs (Brown and London, 1998).

To determine if the presence of M1A in low density fractions is cholesterol dependent, as would be expected for a DRM-associated protein, we treated BBE cells with methyl-β-cyclodextrin (MβCD) to deplete cholesterol. For this experiment, whole cell homogenates (and not crude DRMs) were loaded into the Optiprep™ gradient so that density shifts in the entire cellular distribution of SI and M1A could be observed. The cholesterol profiles from these experiments (Fig. 5 A) revealed the effect of MβCD (solid lines closed square, +MβCD; open squares, −MβCD), demonstrating an ~50% loss of cholesterol in the first fraction. Cholesterol depletion was linked to a significant loss of both SI and M1A from the lowest density fraction (Fig. 5 B, asterisk).

Our density gradient results suggest that M1A and SI coexist in low density fractions in a cholesterol-dependent manner, as would be expected for DRM-associated proteins. To confirm that M1A physically associates with DRMs, we affinity-purified membranes from the crude DRM pool using concanavalin A (ConA), a lectin which binds with high affinity to glycoconjugates such as those found on the extracellular domains of SI (Hauri, 1983). In addition to SI, a substantial fraction of M1A sedimented with ConA-coated, but not uncoated agarose beads (Fig. 5 C). We also attempted to solubilize M1A from the ConA agarose pellet with treatments that would be expected to disrupt DRM structure; e.g., incubation at 37°C or cholesterol depletion. The resulting Western blots (Fig. 5 D) revealed that DRMs in the ConA pellet were rather stable. Although SI would not be expected to release from the ConA resin (as it binds directly and irreversibly), there was almost no release of M1A from the pellet at 37°C and only a small amount of release with MβCD exposure. Thus, although MβCD treatment raises the density of DRMs (Fig. 5, A and B), it may not be stringent enough to abolish lipid raft complexes from BBE cells. This is consistent with recent studies showing that microvillar lipid rafts are much more resistant to high temperature (37°C) and cholesterol extraction when compared with traditional, caveolin-containing rafts (Danielsen and Hansen, 2003). Conversely, if MβCD treatment is disrupting raft structures, these data may indicate that M1A interacts with SI on the surface of the raft (either directly or indirectly); i.e., because SI is bound directly to the ConA resin, an interaction with M1A might stabilize its presence in the pellet despite the disruption of associated lipid components.

## M1A is a component of native SI-containing DRMs isolated from rat MV

In an effort to confirm the presence of M1A in SI-containing DRM fractions from native intestinal epithelia, we pro-

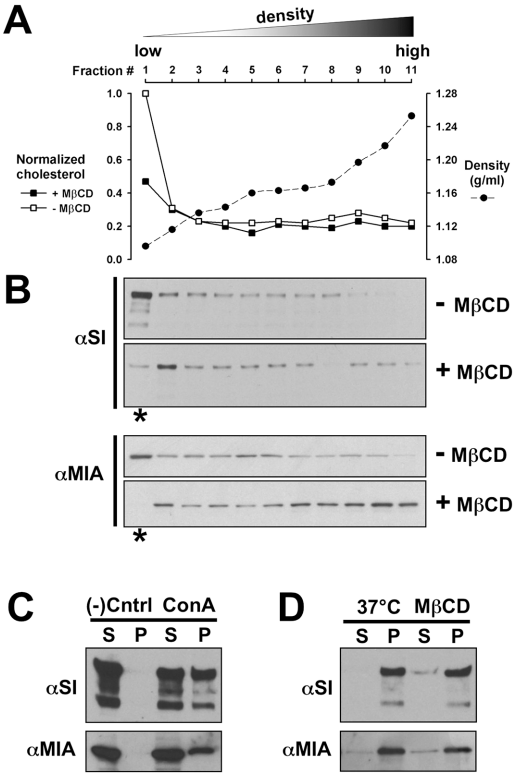


Figure 5. **Effect of MβCD on DRMs isolated from BBE cells.** (A) Density (dashed line, closed circle) and cholesterol profiles of Optiprep™ density gradients used to characterize DRMs from BBE cells with (solid line, filled square) or without (solid line, open square) MβCD treatment. (B) Immunoblots of gradient fractions (loaded for equal volume) demonstrate that cholesterol depletion is linked to a significant loss of SI and M1A from the lowest density fraction (asterisks). (C) Immunoblots of pellet and supernatant fractions from ConA pulldown experiments show that SI and M1A sediment with ConA-coated (ConA), but not uncoated (−Cntrl) agarose beads. (D) Immunoblots reveal that exposure of the ConA pellet (from C) to elevated temperature (37°C) or MβCD (see Materials and methods) results only in minor solubilization of M1A.

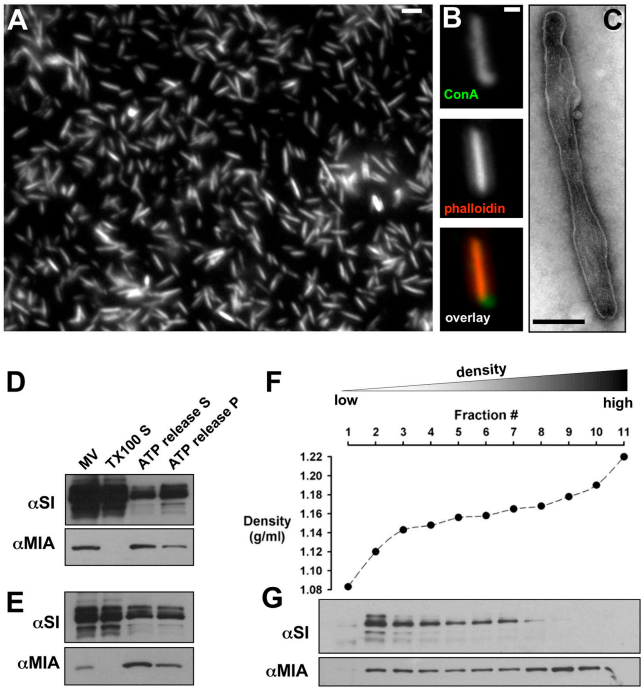


Figure 6. **Characterization of DRMs isolated from rat MV.** (A) Light micrograph of a phalloidin-stained microvillar preparation. Bar, 1 μm. (B) The intact apical membranes associated with purified MV are seen with phalloidin (red) and ConA (green) costaining (Bar, 250 nm) and negative stain (C; Bar, 250 nm). Immunoblots of fractions from the native DRM preparation loaded (D) stoichiometrically (relative to MV volume) or (E) for equal protein; MV, purified microvilli; TX100 S, Triton X-100 solubilized supernatant; ATP release S, post-ATP 40,000 *g* supernatant; ATP release P, post-ATP 40,000 *g* pellet. (F) Density profile of Optiprep™ gradient used to characterize native DRMs. (G) Immunoblots of gradient fractions (loaded for equal volume) probed for SI and M1A.

ceeded to isolate DRMs from rat intestinal MV (Fig. 6 A; Mooseker et al., 1989). Light microscopy on ConA/phalloidin costained samples (Fig. 6 B) and EM on negatively stained preparations (Fig. 6 C) enabled us to verify that MV were purified with apical membranes intact. To isolate DRMs, MV were first demembranated with cold 1% Triton X-100 (see Materials and methods). Immunoblots of the fraction solubilized during this treatment (Fig. 6 D, TX100 S; Table I) showed that a significant portion (~60%) of microvillar SI was released with cold Triton X-100, a finding consistent with previous reports (Danielsen, 1995). This implies either that many of the rafts present at the time of detergent treatment do not "survive" the extraction or that SI exists in equilibrium between raft- and nonraft-associated forms in the microvillar membrane. Demembranated microvillar cores were then resuspended in saturating ATP to release M1A and any associated complexes (e.g., DRMs). M1A in the resulting "ATP release supernatant (S)" fraction was enriched 2.6-fold relative to intact MV (Fig. 6 E; Table I). To determine if M1A in this fraction was present on low density, SI-containing DRMs, we performed density gradient analysis. M1A was distributed throughout the gradient in both low and high density fractions, suggesting that the ATP release S input contained both DRM- and non-DRM–associated (soluble) M1A populations. Densitometric analysis of the immunoblots (Fig. 6 G) revealed that a significant portion (~14%; Table I) of the total M1A input was found in the lowest density fraction that was enriched in SI (Fig. 6, F and G, Fraction 2, ~1.12 g/ml). Because the ATP release S gradient input contains ~76% of the total microvillar M1A (Table I), this translates into a value of ~10% for the amount of M1A that is associated with lowest density DRMs in the MV. However, 10% is a conservative estimate given that a large fraction of SI tails into higher densities (Fig. 6, F and G). If we consider all the fractions that have significant levels of SI (Fig. 6, Fractions 2–7), these also contained ~60% of the M1A from the ATP release S input (Table I).

To further characterize the native DRMs from our microvillar preparation, we performed EM on highly purified DRM fractions (see Materials and methods; Fig. 7 A). These images revealed the presence of "disks," ranging from 100–200 nm in diameter, that were morphologically similar to the M1A-enriched DRM disks isolated from chicken intestinal MV (Mooseker et al., 1989). In some cases, disks exhibited a "rolled edge" (Fig. 7 A, asterisk) indicating that these structures represent sheets of membrane rather than vesicles.

Table I. **Distributions of M1A and SI in fractions from a typical native DRM preparation**[a]

| | M1A | SI |
|---|---|---|
| Biochemical fractions as % of MV total[b] | | |
| TX100 S | – | 59 |
| ATP release S | 76 | 18 |
| ATP release P | 24 | 23 |
| Fold enrichment relative to MV fraction | | |
| TX100 S | – | 0.9 |
| ATP release S | 2.6 | 0.5 |
| ATP release P | 1.6 | 0.3 |
| Density gradient fractions as % of input | | |
| Fraction 2 | 14 | 31 |
| Fractions 2–7 | 60 | 94 |

[a]Determined using densitometric analysis of blot film images.
[b]MV total was obtained from the sum of TX100 S, ATP release S, and ATP release P signals.

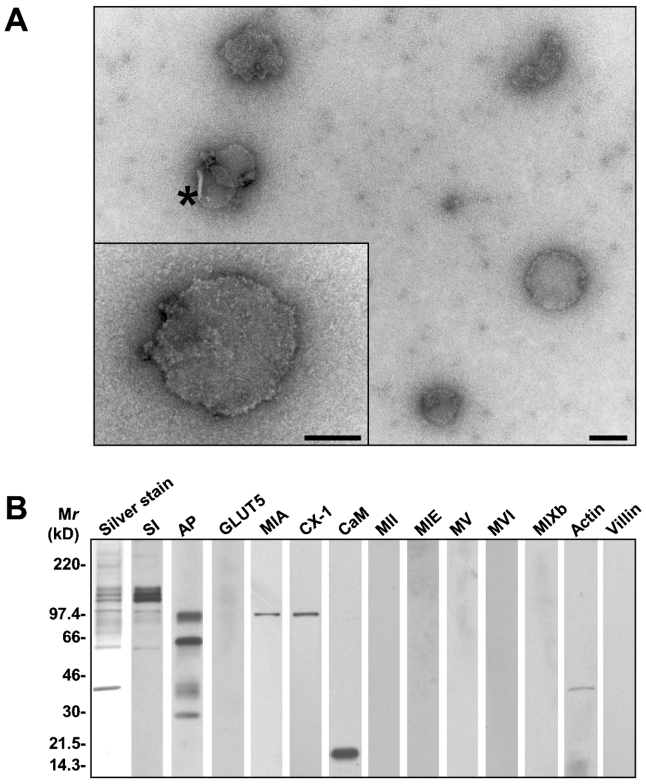


Figure 7. **Native DRMs are isolated as membrane disks.** (A) Negatively stained preparation of highly purified DRMs from the ATP release S fraction (see Materials and methods) reveals the presence stable membrane disks. The asterisk marks a rolled edge on one membrane indicating that these structures are purified as sheets and not vesicles. The inset shows a higher magnification view of a single membrane. Bars, 100 nm. (B) Silver-stained sample and immunoblots of highly purified DRMs with antibodies against SI, AP, glucose transporter-5 (GLUT5), M1A, CX-1 immunogens, CaM, myosin-II (MII), myosin-1E (M1E), myosin-V (MV), myosin-VI (MVI), myosin-IXb (MIXb), actin, and villin.

Most importantly, the disks observed here confirm the existence of intact membrane structures (i.e., DRMs) in our native preparation. Immunoblots on highly purified DRMs (Fig. 7 B) showed that, in addition to SI and M1A, this fraction also contains AP, CaM, and actin. Other common BB components such as villin and myosin-II, along with many other unconventional myosins were absent. The presence of a single CX-1 immunogen at ~110 kD suggests that M1A is the only class I myosin in this fraction.

### M1A interacts with SI on DRMs released from rat MV

To confirm that M1A physically interacts with DRMs from our microvillar preparation, we used ConA-coated beads to affinity purify these membranes from the ATP release S fraction. Most of the SI in this fraction sedimented with ConA-coated, but not uncoated (−Cntrl) beads (Fig. 8 A). A significant fraction of M1A was also found in the ConA pellet, suggesting that this motor physically interacts with glycoconjugate-rich DRMs from this native preparation. To establish that M1A and SI actually coexist on the same membrane structures, we immunopurified (IP) SI-containing DRMs from the ATP release S fraction. Immunoblots of nonimmune IgG and anti-SI IP pellets (Fig. 8 B) showed that SI and M1A are both found in the same subset of DRMs. The presence of M1A was further verified by the coIP of CaM and a single CX-1 immunogen at ~110 kD. The presence of AP in the ConA pellet (Fig. 8 A) and in the anti-SI IP pellet (Fig. 8 B) suggests that intact "whole" DRMs were sequestered in both assays.

To determine if M1A interacts with the cytoplasmic domain of SI while associated with native DRMs, we chemically cross-linked proteins in the ATP release S fraction with the zero-length cross-linker 1-ethyl-3-(3-dimethylaminopropyl) carboiimide (EDC). After the separation of cross-linked products with SDS-PAGE, immunoblotting revealed a high molecular weight product that was positive for SI, M1A, and CaM, but not AP (Fig. 8 C, arrowhead). Given the approximate molecular weight of the cross-linked product (~300 kD), we propose that it represents a single M1A molecule with a complement of CaM light chains, cross-linked to the transmembrane subunit (i.e., isomaltase) of SI. Although these results suggest that M1A and SI interact in a complex on the surface of DRMs, they do not allow us to differentiate between a direct interaction or indirect binding that might be mediated through a third, unknown component. However, any additional component would have be very low mol wt, given that much of the mass (~300 kD) can already be accounted for by proteins identified in Western blots (e.g., the transmembrane subunit of SI, ~140 kD; M1A, ~110 kD; and CaM, ~17 kD × 3).

### Expression of the SI cytoplasmic domain induces the loss of SI from the BB

On the cytoplasmic face of the microvillar membrane, the only portion of SI available for cross-linking to M1A is its small $NH_2$-terminal cytoplasmic domain (SINT) consisting of ~10 aa (Hunziker et al., 1986). If an interaction between M1A and the SINT (be it direct or indirect) is required for the localization of SI-containing DRMs in the BB, expression of this fragment should result in a phenotype similar to that produced by GFP-M1A-tail. To test this proposal, we expressed SINT fused to YFP in BBE cells and examined its effect on SI localization. BBE cells expressing SINT-YFP ex-

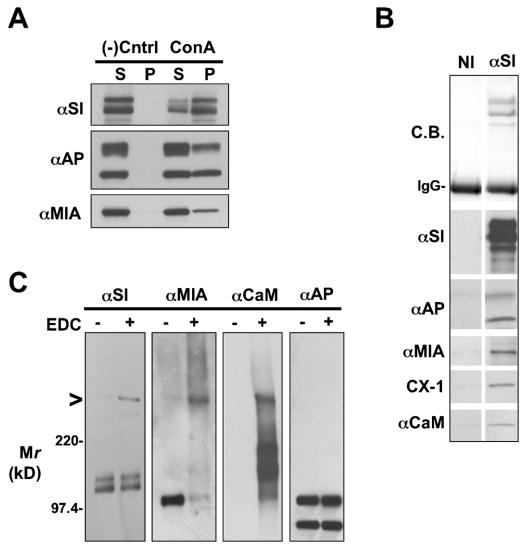


Figure 8. **M1A forms a complex with SI-containing DRMs.** (A) Immunoblots of pellet and supernatant fractions from ConA pulldown experiments show that SI, AP, and M1A are all found on DRMs affinity purified with ConA-coated (ConA), but not uncoated (−Cntrl) agarose beads. (B) Immunopurification of DRMs with αSI shows that M1A, a single CX-1 immunogen (presumably M1A), CaM, and AP all copurify with these membranes; NI is the nonimmune IgG negative control; CB is a Coomassie blue–stained gel. (C) Zero-length chemical cross-linking of the ATP release S fraction with EDC produces a high molecular weight product (∼300 kD, see arrowhead) that is positive for SI, M1A, and CaM, but not AP.

hibited a striking loss of SI from the BB domain (Fig. 9, A and B), an effect similar to that induced by GFP-M1A-tail. This effect was specific to SI as distributions of the other apical membrane markers, APN (Fig. 9 C) and AP (Fig. 9 D), appeared normal. However, in cells expressing high levels of SINT-YFP, we also observed that M1A levels were reduced (Fig. 9 E). Although the effects on M1A were not as pronounced as the impact on SI localization, this result does suggest that the SINT may play a role in docking a fraction of M1A to the microvillar membrane in these cells. The limited effect of SINT-YFP expression on M1A localization is also consistent with our biochemical data on native DRMs, which indicates that as little as ∼10% of the M1A may be DRM-associated in the MV (Fig. 6 G; Table I).

We also performed a quantitative analysis of the effect of SINT-YFP expression by plotting the paired SI and SINT-YFP intensities from 477 BBs (Fig. 10 A). The resulting plot shows that the staining patterns of the two are almost mutually exclusive; SI is only present in the BB at high levels when there is little or no SINT-YFP expression in that particular cell. When this analysis was performed on micrographs of BBE cells expressing GFP-M1A-tail ($n$ = 400), the resulting plot was very similar (Fig. 10 B) suggesting the two dominant negative fragments phenocopy each other with respect to their effect on SI localization. We propose that these dominant negative results, together, reflect the functional significance of the M1A/SI-lipid raft complex identified in our biochemical experiments (Figs. 4–8) and suggest that the interaction between M1A and SI-containing lipid rafts is critical for the proper localization of SI in the BB.

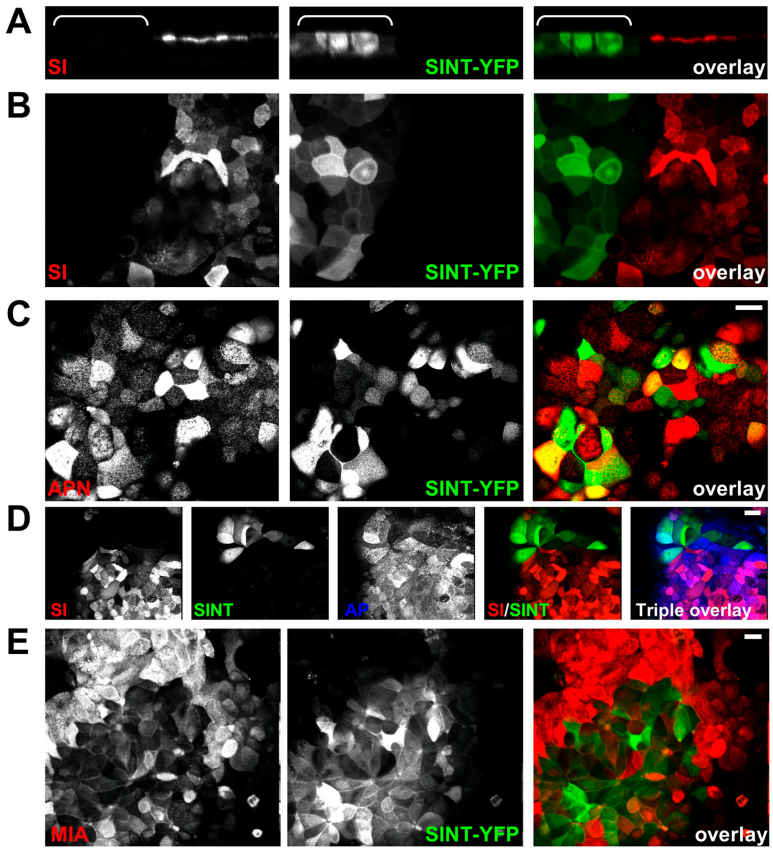


Figure 9. **SI is lost from the BB in cells expressing SINT-YFP.** (A) Vertical and (B) en face confocal sections demonstrate the loss of SI from the BB in cells expressing SINT-YFP. The white bracket in A highlights a cluster of cells expressing high levels of SINT-YFP and lacking SI localization in the BB. (C) En face confocal sections show that APN localizes in the presence of SINT-YFP. (D) SI and AP double staining reveals that AP localizes properly in cells where SINT-YFP has perturbed SI localization. (E) En face confocal sections demonstrate that levels of M1A in BBE cells expressing SINT-YFP are significantly reduced. In the overlay images, GFP signals are green, M1A, SI, and APN are red, AP is blue. Bars, 20 μm.

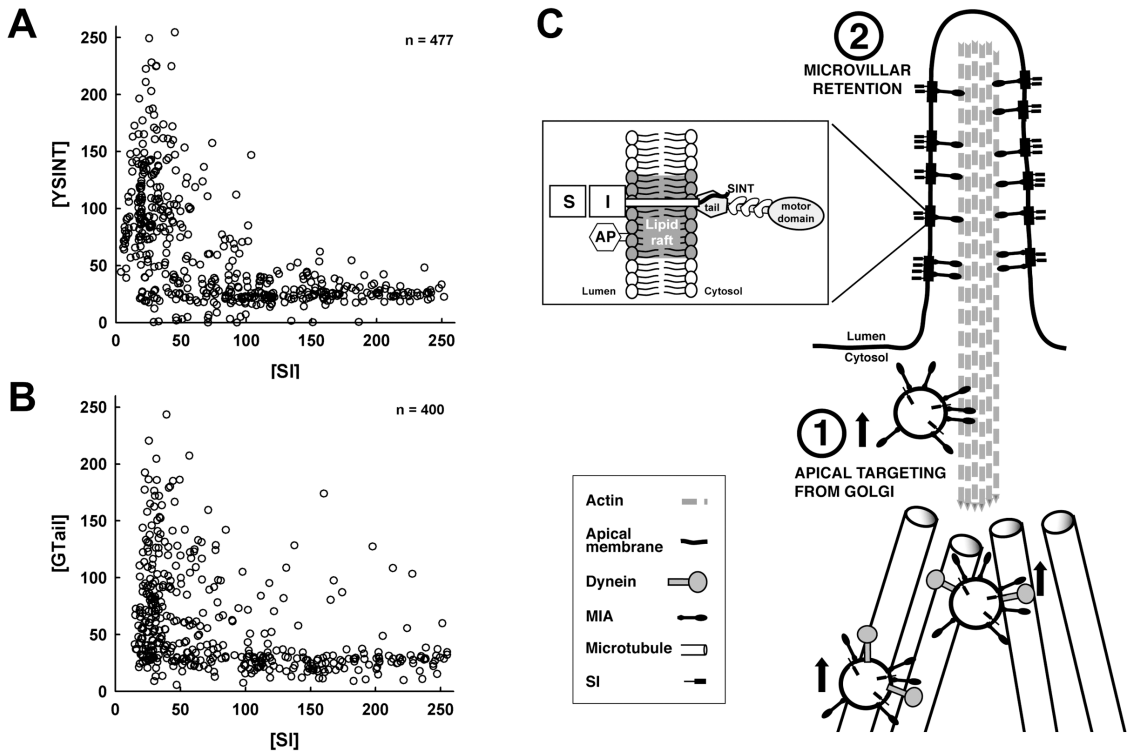


Figure 10. **SINT-YFP and GFP-M1A-tail phenocopy with respect to SI localization.** Plots of the paired intensities of (A) SI and SINT-YFP or (B) SI and GFP-M1A-tail demonstrate that these two fragments phenocopy each other in terms of their effects on SI localization. (C) Two models for M1A function based on the results described here: (1) M1A may power the apical movement of Golgi-derived vesicles laden with SI; or (2) M1A might be responsible for the retention or stabilization of SI in lipid rafts of the BB membrane. The inset is a cartoon depicting the association of M1A with SI-containing lipid rafts. This association may be mediated through a direct interaction between M1A tail domain and the SINT of SI (as shown) or indirectly through a third, unidentified factor.

## Discussion

Here, we describe the association of M1A with SI-containing lipid rafts, as revealed in both an IEC line and in MV isolated from native intestinal epithelia (Figs. 4–8). We also demonstrate that M1A and SI can be cross-linked in a lipid raft complex at zero length (Fig. 8 C). The biological significance of such a complex is reinforced by experiments in BBE cells, which show that the expression of either GFP-M1A-tail (Fig. 3) or SINT-YFP (Fig. 9) abolishes SI localization in the BB (Fig. 10, A and B). Together, these data suggest two potential roles for M1A with regard to SI localization: (1) M1A acts as a motor powering the transport of SI-containing lipid rafts up to the BB (Fig. 10 C, model 1); or (2) M1A is required for the stabilization and/or retention of the SI-lipid raft complex after its delivery to the BB (Fig. 10 C, model 2). At present, the majority of evidence supports model 2.

SI is a type-II integral membrane disaccharidase involved in carbohydrate processing in the intestinal lumen. In vivo SI exists in two forms: a heavily glycosylated 260-kD pro-SI peptide that targets to the apical surface and, once exposed to the intestinal lumen, a dimer that is formed from the tryptic cleavage of pro-SI into sucrase and isomaltase subdomains (Hunziker et al., 1986). In the BB membrane, SI resides in lipid rafts; detergent-resistant microdomains that are known to be rich in sphingolipids and cholesterol, as well as GPI-linked and other transmembrane proteins (Brown and London, 1998). Intriguingly, rafts may also play a role in the sorting of Golgi-derived membrane to the apical surface (Ikonen and Simons, 1998). It is tempting to speculate that the loss of SI from the BB in the presence of GFP-M1A-tail or SINT-YFP may be due to a defect in the trafficking of Golgi-derived lipid rafts (Fig. 10 C, model 1). In this scenario, vesicles coming from the Golgi would be transported by dynein along microtubules to the terminal web region, at which point M1A would power actin-based motility up into the BB (Fath et al., 1994). If M1A interacts with SI on the surface of lipid rafts, expression of both dominant negative fragments would inhibit M1A from binding to such vesicles, and thus prevent the apical transport of SI-containing rafts. In support of this proposal, the intestine of developing mouse embryo exhibits supra-nuclear M1A staining that may represent Golgi-associated motor (Skowron and Mooseker, 1999). Moreover, Jacob et al. (2003) have recently reported that exogenously expressed SI and a myosin identified as M1A, coimmunoprecipitate from a Golgi-enriched vesicle fraction derived from MDCK cells. However, it is unlikely that the Golgi-associated myosin-I immunogen in these studies is actually M1A. Immunoblots of kidney tissue (Skowron et al., 1998) and MDCK cells using our antibody failed to detect M1A although both do express multiple CX-1 reactive immunogens (unpublished data).

The preponderance of evidence indicates that M1A does not power the apical transport of SI-containing vesicles in IECs. The association of M1A with the Golgi, alluded to above, is only observed in undifferentiated enterocytes (Fath

et al., 1994; Skowron et al., 1998), not in differentiated cells of the villus, where synthesis and apical transport of SI must occur given the turnover rates for BB disaccharidases (James et al., 1971). Moreover, in BBE cells expressing GFP-tagged full-length M1A, this motor does not label a population of moving vesicles (unpublished data). The proposed role of the MV core rootlets as tracks for vesicle transport, through the terminal web to the plasma membrane, is also unlikely given that these structures are coated with tropomyosin (Bretscher and Weber, 1978), an actin-binding protein known to inhibit the activity of M1A (Fanning et al., 1994) and other class I myosins (Tang and Ostap, 2001). Tropomyosin also coats the stable actin bundles found in the stress fibers that are commonly observed in unpolarized cells (Tang and Ostap, 2001). Thus, the recently reported movement of SI-containing vesicles along stress fibers (Jacob et al., 2003) is most likely powered by a nonclass I myosin. Finally, the localization of APN (a type II transmembrane raft component; (Danielsen, 1995) and AP (a GPI-linked protein that resides in the same lipid rafts as SI; Garcia et al., 1993), is normal in BBE cells expressing GFP-M1A-tail and SINT-YFP (Figs. 3 and 9). Although it remains possible that APN and AP utilize sorting mechanisms distinct from SI (e.g., M1A independent vs. dependent) to arrive at the apical domain, all of these data together suggest that M1A participates in a process other than motor-driven apical transport.

We propose that M1A is responsible for the retention of SI within BB, specifically through an interaction with SI-containing lipid rafts (Fig. 10, model 2). This interaction would provide a link from SI to the underlying cytoskeleton, stabilizing its residence and extending its lifetime in the BB membrane. Cytoskeletal interactions are known to be critical for the stable localization of other membrane-associated proteins as well. For example, retention of the $Na^+/K^+$ ATPase in the basolateral membrane of enterocytes is known to be dependent on its binding to the underlying meshwork of ankyrin and spectrin (Nelson and Veshnock, 1987). Indeed, previous reports have shown that with respect to $Na^+/K^+$ ATPase localization, phenotypes associated with β-spectrin mutations in *Drosophila* (Dubreuil et al., 2000) are similar to those observed in this work. Here, we observed that the loss of cytoskeletal linkages (induced by expression of GFP-M1A-tail or SINT-YFP, Figs. 3 and 9, respectively) results in a profound loss of SI from the BB with little redistribution to other subcellular compartments. In the absence of cytoskeletal linkages, SI may be more susceptible to removal from the cell via the continuous apical membrane shedding that occurs at microvillar tips in BBE cells (that is, SI is physically lost from the cells). Alternatively, disruption of cytoskeletal linkages may leave SI more susceptible to retrieval from the BB via constitutive endocytic pathways. Once internalized, mislocalized SI would experience a higher rate of degradation. Both of these scenarios could lead to the reduced steady-state SI levels and significantly lower staining intensities observed here.

Are the low duty ratio kinetics (Jontes et al., 1997) and rapid turnover dynamics (Tyska and Mooseker, 2002) reported for M1A consistent with a role in microvillar retention? The unloaded duty ratio of M1A is only ~0.1 (Jontes et al., 1997), suggesting that many molecules (at least 10, ~1/duty ratio), working together in an ensemble, would be required to form a continuous link between the membrane and the microvillar actin core. One way for M1A to form an ensemble might be through the assembly of lipid rafts in the microvillar membrane. In this scenario, the clustering of *n* SI molecules in a single lipid raft would provide *n* docking sites for M1A on the cytoplasmic face. By providing a platform for the formation of a small M1A ensemble, lipid rafts may eliminate the low duty ratio limitation (provided that $n \geq 10$) and allow the multiple SI molecules in a given raft to maintain a continuous link to the underlying cytoskeleton. Alternatively, because the kinetics of M1A may be strain dependent (Jontes et al., 1997), its duty ratio may range from ~0.1 (in the unloaded case) to much higher values in the presence of load (e.g., a stable interaction with SI). Thus, a single M1A molecule, with appropriate loading, might be capable of retaining SI in the absence of a larger motor cluster. Moreover, although FRAP studies have demonstrated that most of the M1A in the BB exchanges rapidly, these data also indicate that a smaller population does not turnover on the time scale of the observations (Tyska and Mooseker, 2002). We speculate that this "immobile" fraction may represent lipid raft-associated M1A engaged in microvillar retention. In support of this hypothesis, our biochemical data indicate that 10–20% of the total microvillar population of M1A associates with SI-containing lipid rafts, a fraction that is similar in magnitude to the immobile fraction provided by FRAP studies (9–23%; see Table I; Tyska and Mooseker, 2002).

M1A was discovered as the first vertebrate class I myosin over a decade ago (Cheney and Mooseker, 1992); the investigation we present here is the first to define a specific function for this motor. In combination with other available evidence, our data suggest that M1A is involved in the retention of SI in the BB, most likely through an interaction with SI-lipid raft complexes. These findings also complement a recent proteomic study that highlighted myosin-1G as a component of DRMs from neutrophils (Nebl et al., 2002). Given that myosins-I are ubiquitously expressed, we predict that future studies will reveal that these motors are lipid raft components in a variety of cell types. Because lipid rafts are thought to function as dynamic signaling platforms with the ability to recruit or exclude specific components based on their biochemical environment and/or extracellular stimuli, future studies will focus on identifying factors that might regulate the interaction between M1A and SI-containing lipid rafts in the MV.

## Materials and methods

### Cell culture

BBE cells were cultured as described previously (Peterson and Mooseker, 1992). Preconfluent BBE cells were maintained in DME (GIBCO BRL) supplemented with 10% FBS (Hyclone), 1× penicillin-streptomycin-fungizone (GIBRO BRL), and 30 μg/ml transferrin (Sigma-Aldrich) at 37°C and 10% $CO_2$. For all light microscopy studies, confluent BBEs were grown on Transwell-COL collagen-coated filters (Corning-Costar) for at least 3 wk to ensure that cells were fully differentiated. For studies involving cholesterol depletion, cells were incubated in 2% MβCD in serum-free DME (Sigma-Aldrich) for 30 min before fractionation.

### Cloning of GFP-M1A-tail and SINT-YFP fusion constructs

The GFP-M1A-tail and SINT-YFP fusion constructs were assembled using standard molecular biological techniques. To fuse GFP to the COOH-terminal tail of M1A (aa 772–1043, Tail), PCR with the full-length human M1A

cDNA (Skowron et al., 1998) as template was used to create a fragment with 5′ XhoI and 3′ XmaI sites that allowed for ligation into the pEGFP-C1 polylinker. Next, PCR was used to create a GFP-M1A-tail fragment with 5′ SalI and 3′ ClaI sites that allowed for ligation into the polylinker of the retroviral vector pLNCX2 (CLONTECH Laboratories, Inc.). To create the dominant negative fragment SINT-YFP, an oligo with 5′ SacI and 3′ XmaI sites encoding the sequence MARKKFSGLE-GG (the 10 $NH_2$-terminal cytoplasmic residues of human SI and a double-glycine linker) was annealed with its reverse complement, cut and ligated into the pEYFP-N1 polylinker.

### Transfections and retroviral infections

Standard transfection protocols recommended for Lipofectamine 2000 (GIBCO BRL) were used to generate BBE stable lines expressing SINT-YFP, whereas stable lines expressing GFP-M1A-tail were generated with a retroviral system. In both cases stable integration was necessary because these cells are grown at confluency for several weeks to achieve a fully differentiated state. To generate recombinant retrovirus for the purpose of infecting BBE cells, PT67 packaging cells (CLONTECH Laboratories, Inc.) at 70–80% confluency were transfected with pLNCX2-GFP-M1A-tail using Lipofectamine 2000 (GIBCO BRL). 48 h after transfection, cells were replated and grown in maintenance medium supplemented with 1 mg/ml G418 (GIBCO BRL) for 2 wk. Media supernatants from virus-producing PT67 cultures were filtered with a low protein-binding (0.04 μm) syringe filter, supplemented with 5 μg/ml hexadimethrine bromide (Sigma-Aldrich), and used to infect preconfluent BBE cells. Stable BBE transformants were selected with 1 mg/ml G418. For these studies, GFP-M1A-tail expressing cells were compared with neighboring cells that demonstrated very low or no expression. This approach was useful as it provided an internal control for variability induced by G418 selection or differences in differentiation state. None of the phenotypes described in this work were observed in cells transfected with EGFP or EYFP alone.

### Immunofluorescence staining

Fully differentiated BBE cells grown on filters (Corning-Costar) were fixed using the pH-shift fixation protocol originally described by Bacallao and Stelzer (1989). In brief, cells were rinsed with prewarmed buffer 6.5 (80 mM K-Pipes, 5 mM EGTA, 2 mM $MgCl_2$, pH 6.5) and then fixed with 3% PFA in buffer 6.5 for 5 min at RT. After aspirating the initial fix, cells were then fixed with 3% PFA in buffer 11 (100 mM $NaB_4O_7$, pH 11.0) for 10 min at RT. Cells were then rinsed twice in PBS, pH 8.0, and incubated with 1 mg/ml $NaBH_4$ in PBS for 15 min. After a thorough rinsing in PBS, cells were permeabilized in 0.1% Triton X-100 for 5 min and blocked in 10% BSA for 20 min. Incubation in primary antibodies for 45 min at 37°C was followed by several washes in PBS, and then incubation in secondary antibodies with the appropriate phalloidin conjugate (1:200) for 20 min at RT. After a final series of washes, filters were cut out of plastic supports, mounted with Citifluor antifade reagent (Ted Pella, Inc.), and stored at 4°C until imaging.

### Antibodies for immunofluorescence

The following primary antibodies and corresponding dilutions were used: anti–human M1A-tail pAb (Skowron et al., 1998), 20 μg/ml; anti–human APN mAb, 1:200 (Biosource International); CX-1, an mAb raised against chicken M1A that recognizes the head domain of multiple myosins (Carboni et al., 1988), 1:100 dilution of ascites fluid; anti-AP polyclonal, 1:500 (Sigma-Aldrich); anti–human SI mAb (a gift from A. Quaroni, Cornell University, Ithaca, NY), 1:500. Secondary antibodies or phalloidin conjugated to either Alexa-488 or Alexa-568 (Molecular Probes) were used at 1:500.

### Light microscopy

All confocal images were acquired on a laser scanning confocal microscope (model MRC-1024; Bio-Rad Laboratories) using 40×/1.0 or 63×/1.4 Plan Apochromat objectives (Carl Zeiss MicroImaging, Inc.). Still images of fixed cells in the plane parallel to the coverslip surface (*x-y*) were acquired by Kalman (Bio-Rad Laboratories) averaging three to five scans with the scan rate to normal. All en face images were taken at the level of the BB. Vertical sections (*z*) were scanned with resolution set to high and scan rate set to normal. Two-color images were acquired with sequential scanning. Images were LUT stretched, pseudo-colored, and overlaid using Metamorph (v. 5.0; Universal Imaging Corp.), and then assembled into figures using Photoshop (v. 5.5; Adobe) or PowerPoint (v. X; Microsoft). For the paired-intensity analysis used to assess the effects of GFP-M1A-tail and SINT-YFP expression on SI localization, Metamorph was used to LUT stretch images so that the 8-bit grayscale values in both channels ranged from 0 to 256 with minimal saturation. The average intensities of both signals for a given cell were recorded and then plotted as coordinates (v. 7.0; Sigmaplot) to determine the degree of correlation.

### SDS-PAGE and immunoblotting

Protein fractions were analyzed with SDS-PAGE using 5–20% gradient gels. For immunoblotting, gels were transferred to nitrocellulose (85 V, 3.5 h) at 4°C. Stock solutions of affinity-purified primary antibodies were diluted 1:1,000 before use and immunogens were visualized using the ECL method according to the manufacturer's instructions (Amersham Biosciences). Primaries used in this study that were not mentioned above include anti-GLUT5 (Calbiochem), anti-CaM mAb (Upstate Biotechnologies), anti–myosin-IE (Skowron et al., 1998), anti–myosin-VI (Hasson and Mooseker, 1994), anti–myosin-V (Suter et al., 2000), anti–myosin-IXb (Wirth et al., 1996), anti-actin mAb (Sigma-Aldrich), and anti-villin mAb (AMAC).

### Preparation of DRMs from BBE cells

Confluent BBE cells were rinsed three times with TBS at 37°C, scraped from the flask, and pelleted (1500 *g*, 10 min). Subsequent steps were performed at 4°C. Cells were resuspended in nine pellet volumes of buffer 2xA′ (2 mM EGTA, 150 mM KCl, 5 mM $MgCl_2$, 1 mM DTT, 1 mM Pefabloc, 40 mM imidazole, pH 7.2) supplemented with 1 mM ATP and 1% Triton X-100, and then homogenized in a stainless steel dounce (Fig. 4 A, Hmg). The postnuclear supernatant (~2 ml; Fig. 4 A, PNS) from this homogenate was underlayed with 1 ml 48% OptiPrep™ (Sigma-Aldrich) and spun at 100,000 *g* for 60 min at 4°C in a Beckman TLA 110 rotor. Crude DRMs were collected from the OptiPrep™ cushion (Fig. 4 A; Interface) and resuspended to 1 ml of 30% OptiPrep™ with 2xA′ and 60% Optiprep™. Density gradients were generated by spinning the resuspended DRMs at 350,000 *g* for 2 h at 4°C in a Beckman TLA 120.2 rotor. Gradient fractions (11 × 90 μl) were taken and subject to cholesterol determination with the Amplex Red assay (Molecular Probes), density determination with a refractometer (model 334610; Bausch & Lomb), SDS-PAGE, and immunoblot analysis as described above.

### Preparation of DRMs from rat MV

BBs were purified from rat small intestine as described elsewhere (Keller and Mooseker, 1982). Microvillar purification and subsequent DRM isolation were performed as described by Mooseker et al. (1989). All steps were performed at 4°C. In brief, microvillar pellets (Fig. 6, D and E, MV) were resuspended in buffer A (1 mM EGTA, 75 mM KCl, 5 mM $MgSO_4$, 1 mM DTT, 1 mM Pefabloc, 10 mM imidazole, pH 7.2) supplemented with 1% Triton X-100 and allowed to incubate on ice for 5 min. Demembranated MV were collected by sedimentation at 40,000 *g* for 15 min and washed several times in ~20 vol buffer A with 1% Triton X-100. After the final wash, M1A and DRMs were released from microvillar cores by resuspension in 5 vol of buffer A supplemented with 1% Triton X-100 and 2 mM ATP (Fig. 6, D and E, ATP release S), followed by sedimentation at 40,000 *g* for 15 min (Fig. 6, D and E, ATP release P). For density gradient analysis, the ATP release S fraction was adjusted to 30% OptiPrep™ with 2xA supplemented with 1% Triton X-100 and 2 mM ATP, and 60% OptiPrep™, and then spun at 350,000 *g* for 2 h at 4°C in a Beckman TLA 120.2 rotor. Gradient fractions (11 × 90 μl) were taken and subject to density determination with a refractometer (model 334610; Bausch & Lomb) and SDS-PAGE/immunoblot analysis as described above. Protein concentrations were determined with the BCA assay (Pierce Chemical Co.). To generate a highly purified DRM fraction for EM (Fig. 7), DRMs were sedimented from the ATP release S fraction at 100,000 *g*, then resuspended and subject to density gradient centrifugation as described above. The lowest density fraction with SI (~1.12 g/ml) was taken for negative stain and immunoblotting.

### Affinity purification of DRMs

For the affinity purification of SI-containing DRMs, CL-4B agarose resin with immobilized streptavidin (Sigma-Aldrich) was incubated overnight at 4°C in the presence (ConA beads) or absence (control beads) of 0.5 mg/ml biotin-ConA (Sigma-Aldrich). The next day, beads were washed five times with 2xA′ supplemented with 1 mM ATP and 1% Triton X-100 and added to DRMs in 2xA′ at a final concentration of 10% (vol/vol). After incubating for 4 h at 4°C, beads were washed five times with 2xA′ supplemented with 1 mM ATP and 1% Triton X-100, resuspended in volumes equal to the supernatant, and processed for SDS-PAGE/immunoblotting. To disrupt purified DRMs, aliquots of the ConA agarose (with DRMs bound) were incubated at 37°C for 30 min or at RT with 2% MβCD for 30 min. Bead pellets were then resuspended in volumes equal to the supernatant and processed for SDS-PAGE/immunoblotting.

### Immunopurification of DRMs

SI-containing DRMs from rat MV were immunopurified with an anti–rat SI pAb (a gift from A. Quaroni). The ATP release S fraction (Fig. 6, D and E) was first precleared by incubating with 10% protein-A Sepharose (PAS;

Amersham Biosciences), for 1 h at 4°C. Next, 10% PAS and equal quantities (5 μg) of either anti-SI or nonimmune rabbit IgG (Jackson ImmunoResearch Laboratories) were added to equal volumes of supernatant and samples were incubated overnight at 4°C. The next day, PAS pellets were washed five times with 2xA′ supplemented with 1 mM ATP and 1% Triton X-100, followed by processing for SDS-PAGE and immunoblotting as described above.

### Chemical cross-linking

DRMs released from rat MV as described above were chemically cross-linked by the addition of EDC (Pierce Chemical Co.) to a final concentration of 50 mM and incubation on ice for 10 min, and then RT for an additional 10 min. The reaction was quenched by adding 1 vol of sample buffer supplemented with 500 mM β-mercapto-ethanol. Cross-linked products were separated with SDS-PAGE using NuPage Novex 3–8% Tris-acetate gradient gels (Invitrogen) and processed for immunoblotting as described above.

### Transmission EM

Rat MV and DRMs were negatively stained with 1% uranyl acetate on nitrocellulose, carbon-coated grids that were glow-discharged immediately before use.

The authors would like to thank members of the Mooseker lab for helpful suggestions and Andreas Quaroni for the generous gift of anti-SI antibodies.

This work was supported by National Institutes of Health grants DK-25387 (to M.S. Mooseker), DK-55389 (to Jon Morrow), and National Research Service Award DK-10113 (to M.J. Tyska).

**Note added in proof.** Portions of the data reported here have been published previously in abstract form (Tyska, M.J., and M.S. Mooseker. 2002. *Mol. Biol. Cell.* 13:179a; and Tyska, M.J., and M.S. Mooseker. 2003. *Mol. Biol. Cell.* 14:178a).

Submitted: 7 October 2003
Accepted: 2 April 2004

## References

Bacallao, R., and E.H. Stelzer. 1989. Preservation of biological specimens for observation in a confocal fluorescence microscope and operational principles of confocal fluorescence microscopy. *Methods Cell Biol.* 31:437–452.

Bose, A., A. Guilherme, S.I. Robida, S.M. Nicoloro, Q.L. Zhou, Z.Y. Jiang, D.P. Pomerleau, and M.P. Czech. 2002. Glucose transporter recycling in response to insulin is facilitated by myosin Myo1c. *Nature.* 420:821–824.

Bretscher, A., and K. Weber. 1978. Localization of actin and microfilament-associated proteins in the microvilli and terminal web of the intestinal brush border by immunofluorescence microscopy. *J. Cell Biol.* 79:839–845.

Brown, D.A., and E. London. 1998. Functions of lipid rafts in biological membranes. *Annu. Rev. Cell Dev. Biol.* 14:111–136.

Carboni, J.M., K.A. Conzelman, R.A. Adams, D.A. Kaiser, T.D. Pollard, and M.S. Mooseker. 1988. Structural and immunological characterization of the myosin-like 110-kD subunit of the intestinal microvillar 110K-calmodulin complex: evidence for discrete myosin head and calmodulin-binding domains. *J. Cell Biol.* 107:1749–1757.

Cheney, R.E., and M.S. Mooseker. 1992. Unconventional myosins. *Curr. Opin. Cell Biol.* 4:27–35.

Coluccio, L.M. 1997. Myosin I. *Am. J. Physiol.* 273:C347–C359.

Danielsen, E.M. 1995. Involvement of detergent-insoluble complexes in the intracellular transport of intestinal brush border enzymes. *Biochemistry.* 34:1596–1605.

Danielsen, E.M., and G.H. Hansen. 2003. Lipid rafts in epithelial brush borders: atypical membrane microdomains with specialized functions. *Biochim. Biophys. Acta.* 1617:1–9.

Dubreuil, R.R., P. Wang, S. Dahl, J. Lee, and L.S. Goldstein. 2000. *Drosophila* beta spectrin functions independently of alpha spectrin to polarize the Na,K ATPase in epithelial cells. *J. Cell Biol.* 149:647–656.

Durrbach, A., K. Collins, P. Matsudaira, D. Louvard, and E. Coudrier. 1996. Brush border myosin-I truncated in the motor domain impairs the distribution and the function of endocytic compartments in an hepatoma cell line. *Proc. Natl. Acad. Sci. USA.* 93:7053–7058.

Durrbach, A., G. Raposo, D. Tenza, D. Louvard, and E. Coudrier. 2000. Truncated brush border myosin I affects membrane traffic in polarized epithelial cells. *Traffic.* 1:411–424.

Fanning, A.S., J.S. Wolenski, M.S. Mooseker, and J.G. Izant. 1994. Differential regulation of skeletal muscle myosin-II and brush border myosin-I enzymology and mechanochemistry by bacterially produced tropomyosin isoforms. *Cell Motil. Cytoskeleton.* 29:29–45.

Fath, K.R., G.M. Trimbur, and D.R. Burgess. 1994. Molecular motors are differentially distributed on Golgi membranes from polarized epithelial cells. *J. Cell Biol.* 126:661–675.

Garcia, M., C. Mirre, A. Quaroni, H. Reggio, and A. Le Bivic. 1993. GPI-anchored proteins associate to form microdomains during their intracellular transport in Caco-2 cells. *J. Cell Sci.* 104(Pt 4):1281–1290.

Hasson, T., and M.S. Mooseker. 1994. Porcine myosin-VI: characterization of a new mammalian unconventional myosin. *J. Cell Biol.* 127:425–440.

Hauri, H.P. 1983. Biosynthesis and transport of plasma membrane glycoproteins in the rat intestinal epithelial cell: studies with sucrase-isomaltase. *Ciba Found. Symp.* 95:132–163.

Hayden, S.M., J.S. Wolenski, and M.S. Mooseker. 1990. Binding of brush border myosin I to phospholipid vesicles. *J. Cell Biol.* 111:443–451.

Heintzelman, M.B., and M.S. Mooseker. 1990. Assembly of the brush border cytoskeleton: changes in the distribution of microvillar core proteins during enterocyte differentiation in adult chicken intestine. *Cell Motil. Cytoskeleton.* 15:12–22.

Hunziker, W., M. Spiess, G. Semenza, and H.F. Lodish. 1986. The sucrase-isomaltase complex: primary structure, membrane-orientation, and evolution of a stalked, intrinsic brush border protein. *Cell.* 46:227–234.

Ikonen, E., and K. Simons. 1998. Protein and lipid sorting from the trans-Golgi network to the plasma membrane in polarized cells. *Semin. Cell Dev. Biol.* 9:503–509.

Jacob, R., M. Heine, M. Alfalah, and H.Y. Naim. 2003. Distinct cytoskeletal tracks direct individual vesicle populations to the apical membrane of epithelial cells. *Curr. Biol.* 13:607–612.

James, W.P., D.H. Alpers, J.E. Gerber, and K.J. Isselbacher. 1971. The turnover of disaccharidases and brush border proteins in rat intestine. *Biochim. Biophys. Acta.* 230:194–203.

Jontes, J.D., E.M. Wilson-Kubalek, and R.A. Milligan. 1995. A 32 degree tail swing in brush border myosin I on ADP release. *Nature.* 378:751–753.

Jontes, J.D., R.A. Milligan, T.D. Pollard, and E.M. Ostap. 1997. Kinetic characterization of brush border myosin-I ATPase. *Proc. Natl. Acad. Sci. USA.* 94: 14332–14337.

Keller, T.C., III, and M.S. Mooseker. 1982. $Ca^{++}$-calmodulin–dependent phosphorylation of myosin, and its role in brush border contraction in vitro. *J. Cell Biol.* 95:943–959.

Mooseker, M.S., and R.E. Cheney. 1995. Unconventional myosins. *Annu. Rev. Cell Dev. Biol.* 11:633–675.

Mooseker, M.S., K.A. Conzelman, T.R. Coleman, J.E. Heuser, and M.P. Sheetz. 1989. Characterization of intestinal microvillar membrane disks: detergent-resistant membrane sheets enriched in associated brush border myosin I. *J. Cell Biol.* 109:1153–1161.

Nebl, T., K.N. Pestonjamasp, J.D. Leszyk, J.L. Crowley, S.W. Oh, and E.J. Luna. 2002. Proteomic analysis of a detergent-resistant membrane skeleton from neutrophil plasma membranes. *J. Biol. Chem.* 277:43399–43409.

Nelson, W.J., and P.J. Veshnock. 1987. Ankyrin binding to ($Na^+/K^+$) ATPase and implications for the organization of membrane domains in polarized cells. *Nature.* 328:533–536.

Peterson, M.D., and M.S. Mooseker. 1992. Characterization of the enterocyte-like brush border cytoskeleton of the C2BBe clones of the human intestinal cell line, Caco-2. *J. Cell Sci.* 102:581–600.

Raposo, G., M.N. Cordonnier, D. Tenza, B. Menichi, A. Durrbach, D. Louvard, and E. Coudrier. 1999. Association of myosin I alpha with endosomes and lysosomes in mammalian cells. *Mol. Biol. Cell.* 10:1477–1494.

Skowron, J.F., and M.S. Mooseker. 1999. Cloning and characterization of mouse brush border myosin-I in adult and embryonic intestine. *J. Exp. Zool.* 283: 242–257.

Skowron, J.F., W.M. Bement, and M.S. Mooseker. 1998. Human brush border myosin-I and myosin-Ic expression in human intestine and Caco-2BBe cells. *Cell Motil. Cytoskeleton.* 41:308–324.

Suter, D.M., F.S. Espindola, C.H. Lin, P. Forscher, and M.S. Mooseker. 2000. Localization of unconventional myosins V and VI in neuronal growth cones. *J. Neurobiol.* 42:370–382.

Tang, N., and E.M. Ostap. 2001. Motor domain-dependent localization of myo1b (myr-1). *Curr. Biol.* 11:1131–1135.

Tyska, M.J., and M.S. Mooseker. 2002. MYO1A (brush border myosin I) dynamics in the brush border of LLC-PK1-CL4 cells. *Biophys. J.* 82:1869–1883.

Wirth, J.A., K.A. Jensen, P.L. Post, W.M. Bement, and M.S. Mooseker. 1996. Human myosin-IXb, an unconventional myosin with a chimerin-like rho/rac GTPase-activating protein domain in its tail. *J. Cell Sci.* 109:653–661.